HHS Public Access

Author manuscript

J Comp Neurol. Author manuscript; available in PMC 2015 June 19.

Published in final edited form as:

J Comp Neurol. 2014 February 15; 522(3): 717–729. doi:10.1002/cne.23478.

Ultrastructure of Cisternal Synapses on Outer Hair Cells of the Mouse Cochlea

Paul Albert Fuchs[1,2,*], **Mohamed Lehar**[1], and **Hakim Hiel**[1]

[1]Center for Hearing and Balance, Otolaryngology-Head and Neck Surgery, Johns Hopkins University School of Medicine, Baltimore, Maryland 21205 [2]Center for Sensory Biology, Johns Hopkins University School of Medicine, Baltimore, Maryland 21205

Abstract

C (cisternal) synapses with a near membrane postsynaptic cistern are found on motor neurons and other central neurons, where their functional role is unknown. Similarly structured cisternal synapses mediate cholinergic inhibition of cochlear hair cells via α9α10-containing ionotropic receptors and associated calcium-activated (SK2) potassium channels, providing the opportunity to examine the ultrastructure of genetically altered cisternal synapses. Serial section electron microscopy was used to examine efferent synapses of outer hair cells (OHCs) in mice with diminished or enhanced cholinergic inhibition. The contact area of efferent terminals, the appositional area of the postsynaptic cistern, the distance of the cistern from the plasma membrane, and the average width of the cisternal lumen were recorded. The synaptic cisterns of wild- type OHCs were closely aligned (14-nm separation) with the hair cell membrane and coextensive with the micrometers-long synaptic terminals. The cisternal lumen averaged 18 nm so that the cisternal volume was approximately 30% larger than that of the cytoplasmic space between the cistern and the plasma membrane. Synaptic ultrastructure of α9L9′T knockin OHCs (acetylcholine receptor gain of function) were like those of wild-type littermates except that cisternal volumes were significantly larger. OHCs of SK2 knockout mice had few small efferent terminals. Synaptic cisterns were present, but smaller than those of wild-type littermates. Taken together, these data suggest that the cistern serves as a sink or buffer to isolate synaptic calcium signals. J. Comp. Neurol. 522:717-729, 2014.

INDEXING TERMS

synaptic cistern; calcium store; cholinergic inhibition; cochlea; hair cell

*CORRESPONDENCE TO: Paul Fuchs, Ph.D., 818 Ross Research Building, 720 Rutland Avenue, Johns Hopkins University School of Medicine, Baltimore, MD 21205.pfuchs1@jhmi.edu.

CONFLICT OF INTEREST STATEMENT

The authors declare that there is no conflict of interest.

ROLE OF AUTHORS

All authors had full access to all the data in the study and take responsibility for the integrity of the data and the accuracy of the data analysis. Study concept and design: PF, ML, HH. Acquisition of data: ML, HH. Analysis and interpretation of data: PF. Drafting of the manuscript: PF. Critical revision of the manuscript for important intellectual content: HH. Statistical analysis: PF. Obtained funding: PF.

Mechanosensory hair cells of the vertebrate inner ear are subject to centrifugal control by inhibitory cholinergic neurons. Cholinergic efferent inhibition of cochlear hair cells is mediated by uncommon members of the nicotinic (ionotropic) receptor family acting through associated calcium-gated potassium channels (Wersinger and Fuchs, 2011), a synaptic mechanism not known elsewhere in the vertebrate nervous system. These functional peculiarities are associated with an equally uncommon synaptic structure; the synaptic cistern, lying just under the hair cell membrane in parallel with the efferent synaptic contact. This structure was described in early electron micrographs (Engstrom, 1958; Saito, 1980; Smith and Sjostrand, 1961a) and appears to be an obligatory component of cholinergic synapses on all types of hair cells. Synaptic cisterns in hair cells are similar in appearance to subsurface or hypolemmal cisterns found in various neurons and neuroendocrine cells where they have been postulated to serve as specialized calcium stores (Heinzeller and Tutter, 1991; Kaufmann et al., 2009; Lee et al., 2008; Tutter et al., 1991a, 1991b). Intriguingly, subsurface cisterns found in spinal and cranial motor neurons at “C synapses” are thought to mediate cholinergic transmission (Nagy et al., 1993; Yamamoto et al., 1991). Although not all examples of subsurface cisterns are associated with synaptic contacts, those of outer hair cells (OHCs) provide a particularly detailed model for which the identities of neurotransmitter receptors and associated ion channels are well established. Thus, synaptic structure can be analyzed in mouse models in which identified postsynaptic receptors and ion channels have been altered genetically.

What might be the role of the synaptic cistern? One hypothesis is that the cistern is a calcium source to support the cholinergic activation of calcium-gated potassium channels. Alternatively, and perhaps more likely, the synaptic cistern may serve primarily as a barrier, delimiting a restricted volume for calcium’s action; acting as a sink, the cistern also may prevent the spread of calcium signals between efferent and nearby afferent synapses. In reality, the cistern could be both sink and source of calcium, varying as a function of activity level. The relative importance of storage and release might be distinguished by determining whether synaptic activity causes predicted changes in cisternal structure. In the simplest view, increased activity should fill, and possibly expand, a calcium sink, but shrink, or leave unchanged a calcium store. One caveat is that any such changes are likely to be rapidly reversed during the time required for tissue processing. So, for example, varying duration acoustic trauma seemed to cause no lasting change in synaptic cisterns of cochlear hair cells of rabbits (Omata and Schatzle, 1984). An alternative approach is to examine cisterns in genetically altered mice in which known molecular components of the synapse have been altered to reduce or enhance synaptic function. Such permanent alterations in function might be reflected in structural changes of the synaptic cistern. For example, when the store-associated protein Stim-1 was overexpressed in HeLa cells, near-membrane cisterns became multilayered, producing cisternal stacks (Orci et al., 2009).

Studies in the past two decades have identified several candidate molecular components of efferent synapses on hair cells, in particular the α9 and α10 subunits of the acetylcholine receptor (AChR) (Elgoyhen et al., 1994, 2001) and the SK2 (KCNNA) potassium channel (Dulon et al., 1998) with which the receptor interacts. Efferent inhibition fails in the α9 knockout mouse (Vetter et al., 1999), whereas those of a “gain of function” knockin mouse

have greatly prolonged cholinergic inhibition, and strengthened efferent suppression of cochlear signals (Taranda et al., 2009). Hair cells of the SK2 knockout mouse also lose their cholinergic response, but in addition have greatly disrupted efferent innervation (Kong et al., 2008) and reduced cochlear suppression (Murthy et al., 2009a). These genetic models with distinctive changes in efferent function were studied with electron microscopy. Synaptic cisterns were altered in size and shape in α9 knockin and SK2 knockouts, suggesting a role as a fixed calcium buffer to regulate calcium in the synaptic region. However, synaptic cisterns in α9 knockout hair cells were not significantly different from those of wild-type littermates. Finally, associated increases in afferent innervation of the SK2 null OHCs suggest competitive interactions with efferent contacts.

MATERIALS AND METHODS

Mouse lines

$SK2^{\Delta/\Delta}$ (homozygous knockout in C57BI/6) mice were shown previously to have greatly reduced efferent innervation, no cochlear inhibition, and hair cells that were insensitive to ACh (Kong et al., 2008; Murthy et al., 2009a). The intracellular N-terminal domain and trans-membrane regions one and two were excised from the SK2 coding region, eliminating SK2 expression at the mRNA and protein level in brain tissue of $SK2^{\Delta/\Delta}$ mice (Bond et al., 2004) (Table 1).

$\alpha9^{\Delta/\Delta}$ (homozygous knockout) mice have qualitatively normal efferent innervation, but no cochlear inhibition (Vetter et al., 1999). In the altered gene the ligand-binding site, the first and second transmembrane domains, and a portion of the third transmembrane domain of the α9 coding region were excised. The remaining sequence also cannot be translated due to a frame shift, leaving only 100 amino acids of the extracellular amino terminus. The original mice (129S6) were subsequently backcrossed onto CBA/CaJ.

In $\alpha9^{L9'T/L9'T}$ (homozygous knockin) mice (Taranda et al., 2009) the native α9 coding sequence was replaced with one in which a hydrophobic amino acid (9′ leucine) lining the channel pore is replaced with hydrophilic threonine. This alteration favors the open state of the channel, leading to prolonged open times (Plazas et al., 2005). In the $\alpha9^{L9'T/L9'T}$ mice, efferent synaptic currents decay more slowly, and inhibition of distortion product otoacoustic emissions (reflecting the activity of cochlear OHCs) is greatly enhanced and prolonged (Taranda et al., 2009). These mice were back-crossed (>F10) onto an FVB129.J2 background.

Homozygous knockout and knockin mice and their homozygous wild-type littermates ($\alpha9^{+/+}$, $SK2^{+/+}$ and $\alpha9^{L9/L9}$, respectively) were examined in all cases; genotypes were verified by polymerase chain reaction (PCR) on genomic tail DNA.

Tissue fixation and sectioning

Animals were euthanized according to approved protocols (Johns Hopkins Institutional Animal Care and Use Committee). The animals were placed in an inhalation chamber (Harvard Apparatus, Dover, MA) saturated with isoflurane (IsoSol, Penn Veterinary Supply, Lancaster, PA). The fully sedated animal (unresponsive to foot pinch) was rapidly

decapitated and the temporal bones promptly removed. The otic capsules were immediately opened and 1% osmium (OsO_4), and 1% potassium ferricyanide [$FeK_3(CN)_6$] in 0.1 M sym-collidine-HCI buffer (pH 7.4) was perfused through the round window. The tissue was postfixed for 1 hour, rinsed thoroughly by perfusing 0.1 M maleate buffer (pH 7.4) through the round window, and decalcified with gentle shaking for 48–72 hours at 4°C in 5% EDTA in 0.1 M phosphate buffer (pH 7.4–7.8). Following standard protocols, the cochleae were processed for embedding into Araldite. Sections (40 μm) parallel to the modiolus of the whole cochlea were collected and re-embedded in Epon sandwiched between Aclar sheets (EMS, Hatfield, PA). Selected organ of Corti segments from different turns were photographed for record keeping.

Microscopy

Best organ of Corti segments were excised from the 40-μm whole cochlear sections, remounted into Epon blocks, and oriented to achieve ultra-thin sectioning (Leica Ultracut S) parallel to the modiolar axis (perpendicular to the organ of Corti). Serial 65-nm ultra-thin sections were collected onto Formvar-coated slot grids, examined, and photographed on a Hitachi H7600 transmission electron microscope at 80 kV. Once an efferent-OHC contact was identified, it was followed and photographed in consecutive serial ultra-thin sections. Digital images (2,120 × 2,120 pixels) were collected at 8- or 16-bit depth and analyzed as 8-bit files.

Image analysis

Electron micrographs were collected for analysis at magnifications of 30,000–100,000×. Lower power images were collected for orientation. Digital images were imported into Reconstruct software (Fiala, 2005) where montages were assembled and serial sections aligned and calibrated. Line tracings were made of the plasma membranes of hair cells and neuronal contacts. The synaptic cistern was drawn as an enclosed area, as was the region of cytoplasm between the cistern and the plasma membrane (the cytoplasmic gap). In some cases synaptic vesicles and putative active zones of efferent terminals were traced. Hair cell ribbons and associated vesicles were traced when present in the high-magnification images. The volumes of the synaptic cistern and cytoplasmic gap were computed based on a nominal section thickness of 65 nm. The appositional areas of the efferent terminal and synaptic cistern were obtained by tracing a line along their maximum extent in each section, multiplying by the section thickness, and then summing for all sections in the series. This z-axis area was divided into the computed volume to obtain the average width of the cisternal lumen, and that of the underlying cytoplasmic gap.

RESULTS

The data presented here were obtained from the middle ($\alpha9^{L9'T/L9'T}$ [knockin], $\alpha9^{\Delta/\Delta}$ [knockout]) or basal ($SK2^{\Delta/\Delta}$ [knockout]) turns of transgenic mice and their homozygous wild-type littermates (Table 1). Several hundred serial sections were captured from each block, providing 20–40 μm of tissue depth in which to analyze synaptic structures at the base of OHCs. When efferent synapses were found, the entire organ of Corti was imaged at low magnification for orientation and determination of OHC row number (Fig. 1A).

Synaptic cisterns were imaged at higher magnification (30,000–100,000×; Fig. 1B,C). Synaptic cisterns often spanned adjacent efferent terminals, and so reconstructions included all the efferent contacts on each OHC in a given series of sections.

Images of a given synaptic section were assembled into montages, calibrated, and aligned with other sections for serial reconstruction. Drawing tools were used to outline the plasma membranes of the OHC and associated efferent terminals, to trace the perimeter of the synaptic cistern, and the perimeter of the cytoplasmic gap between the cistern and the hair cell plasma membrane (Fig. 2A), as well as any nearby afferent contacts, ribbons, and vesicles. A 3D reconstruction was made from the serial sections. A z-axis projection (Fig. 2B, tilted forward ~30 degrees from the plane of section) illustrates the overlap of the synaptic cistern with the underlying efferent terminal, and the position of a neighboring afferent contact and ribbon. The length of the efferent contact with the hair cell plasma membrane, and the corresponding extent of the synaptic cistern were recorded for each section. Terminal and cistern extent were multiplied by the section thickness (65 nm) and summed to obtain the appositional area for both objects in the Z-dimension. Finally, the cisternal and gap volumes obtained from the 3D reconstruction were recorded, and divided by the appositional area to establish the average cisternal lumen and gap width. The gap and lumenal widths were measured directly on some sections for comparison with the value obtained from 3D reconstruction.

Wild-type efferent synapses in middle and basal turns of the cochlea

Synaptic contacts on a total of 23 partial or complete efferent contacts on 18 OHCs in four homozygous wild-type littermates (all lines) were imaged and reconstructed (Table 1). This constituted a total of 28.4 μm of tissue depth: 15.8 μm from the middle cochlear turn of two $\alpha9^{L9/L9}$ knockin wild types, 2.3 μm from the middle turn of one $\alpha9^{+/+}$ knock-out wild-type, and 10.2 μm from the basal turn of one $SK2^{+/+}$ knock-out wild-type. OHCs in all three rows were analyzed (seven cells from row 1, six from row 2, and five from row 3) with no obvious differences in cisternal structure between rows. Up to four efferent terminals were found on individual OHCs. Single terminals ranged up to 3 μm in maximal extent (individual sections), whereas the average maximal extent was 2.2 ± 1.0 μm. In wild-type OHCs the synaptic cisterns were coextensive with the efferent terminals, both by maximal extent and by appositional area. Synaptic cisterns could be continuous across multiple efferent terminals. The maximal cisternal extent ranged up to 4 μm (covering several efferent terminals), but the average across all synapses was 2.2 ± 1.2 μm. Cisternal dimensions and synaptic appositional areas were similar in all the wild-type OHCs examined (Fig. 3A). The ratio of cisternal area (facing the OHC membrane) to efferent terminal contact area was 0.93 ± 0.14 (n = 20), confirming that cisterns were coextensive with the efferent contact.

The synaptic cistern was tightly and consistently spaced from the OHC membrane (“cytoplasmic gap”; Fig. 3B). The distance of the synaptic cistern from the hair cell plasma membrane was 14.1 ± 1.7 nm (SD, n = 23) among all wild-type OHCs. In many regions the distance between cisternal membranes (lumenal width) appeared to be equivalent to the cytoplasmic separation between cistern and plasma membrane, so that all three membranes

formed nearly parallel lines (the “tram track”; Fig. 1C). In other areas the cisternal lumen varied in width, bulging at the edges and at points where the cistern spanned junctions between efferent terminals (Fig. 4A,B). In some instances secondary or accessory sacs were observed (Fig. 4C, and see Fig. 2A). Sometimes the cistern appeared incomplete (Fig. 4D) and in such circumstances was interpolated between visible points. Such breaks may have been more apparent than real as the membrane curved out of the plane of the section. Accessory sacs were often found in adjacent sections, consistent with this interpretation, although actual breaks in the cisternal membrane cannot be ruled out. Even taking into account these variations, the cisternal volume was only one-third greater (1.29 ± 0.12) than the cytoplasmic volume (“gap”) underlying the cistern (between the cistern and the hair cell’s plasma membrane).

The extensive size of the cistern may be related to the functional organization of the efferent terminals. These are richly endowed with thousands of synaptic vesicles (Fig. 5A – C). Although these spread throughout the terminal, there are also distinct points at which vesicles cluster toward the plasma membrane, often with associated dense material. These areas have the appearance of active zones where vesicles congregate for release into the synaptic cleft. Such putative active zones are scattered throughout efferent terminal (Fig. 5D) so that transmitter release might occur over a wide expanse of the postsynaptic membrane. Given that possibility, it is likely that the synaptic cistern is coextensive with efferent terminals to mediate the effects of widespread neurotransmitter release.

The close, regular spacing of the synaptic cistern is particularly impressive given that this small intermembrane distance is strictly maintained throughout the microns-long extent of the synaptic cistern. In some well-oriented sections it was apparent that the cytoplasmic gap was not homogeneous in appearance, but rather contained periodic variations in density (Fig. 6)-presumably proteinaceous material that binds the metal ions used to provide contrast. An analysis of opacity (staining density) on a line along the cytoplasmic gap shows regular variations (Fig. 6B) with a predominant interval at 16 nm, as determined by Fourier analysis (Fig. 6C). It is not known what molecules staple the cistern in place, but the cytoplasmic gap width was not different in OHCs without SK2 channels or the α9 subunit of the acetylcholine receptor (Fig. 3B).

Cisterns in OHCs of mutant mice α*9 knockin mice (α9$^{L9'T/L9'T}$)*

Efferent synaptic currents in $\alpha9^{L9'T/L9'T}$ (homozygous knockin) hair cells are longer lasting, and efferent suppression of OHC-produced distortion products is exaggerated and considerably longer lasting (Taranda et al., 2009). Thus, this is essentially a gain-of-function mutation of the hair cell AChR. Efferent innervation is present, with subtle alterations in the number and size of contacts on each OHC (Murthy et al., 2009b). Twenty-two synapses on 20 $\alpha9^{L9'T/L9'T}$OHCs were examined (six from row 1, eight from row 2, and six from row 3).

In these OHCs, the cistern to terminal appositional area was 0.90 ± 0.12, similar to that of wild-type littermates (0.95 ± 0.12; Fig. 3A). The synaptic cisterns in $\alpha9^{L9'T/L9'T}$ OHCs differed significantly in only one respect from those of wild-type littermates. The average width of the cisternal lumen (25.5 ± 5.3 nm) was significantly larger ($P = 0.035$, $t = 2.215$, df = 27) than that of wild-type OHCs (20.9 ± 4.8 nm; Fig. 7 and see Fig. 3C). Because the

cytoplasmic gap was not different (15.6 ± 1.6 nm) in the $\alpha9^{L9'T/L9'T}$ animals, compared with that of $\alpha9^{L9/L9}$ wild type littermates (16.1 ± 1.9 nm), the lumen to gap volume ratio was significantly ($P = 0.002$, $t = 3.348$ df = 26) greater in the $\alpha9^{L9'T/L9'T}$ (1.71 ± 0.47) than that of $\alpha9^{L9/L9}$ littermates (1.29 ± 0.19; Fig. 3D). The increased cisternal volume was due in part to expansion of the primary cistern, and in part to more prevalent accessory cisternae (Fig. 7). These varied in size and shape. In some sections a connection to the primary cistern was evident, in others not. Membrane-bound structures were considered secondary cisternae if the parallel separation from the primary cistern was less than or equal to 20 nm. On this basis the cisterns of $\alpha9^{L9'T/L9'T}$ "gain-of-function" synapses were expanded relative to those of wild-type $\alpha9^{L9/L9}$ OHCs.

α9 knockout mice ($\alpha9^{\Delta/\Delta}$)

Without the α9 subunit there is no efferent inhibition of cochlear signaling (Vetter et al., 1999), so that efferent synapses should have little or no activity. Sixteen synapses on 16 $\alpha9^{\Delta/\Delta}$ OHCs were studied (six in row 1, five in row 2, and five in row 3). The ultrastructure of efferent synapses on $\alpha9^{\Delta/\Delta}$ OHCs was not significantly different from that of wild-type littermates, although there was more variability in cisternal volumes than seen in other mouse lines (Fig. 3). Cisterns and efferent terminals averaged 2 μm in maximum extent (individual sections), so that the ratio of appositional areas was 0.96 ± 0.02. The cytoplasmic gap width between synaptic cistern and OHC plasma membrane was 15.9 ± 4.0 nm, not significantly ($P = 0.16$, $t = 1.460$ df = 16) different from that of wild-type littermates (13.9 ± 2.0 nm). The cisternal lumen width in $\alpha9^{\Delta/\Delta}$ OHCs averaged 21.3 ± 7.9 nm, larger but not significantly ($P = 0.33$ $t = 1.012$ df = 16) different from that of wild- type littermates (17.5 ± 4.0 nm). The cisternal to cytoplasmic volume ratio (1.33 ± 0.4) was statistically the same as that of wild-type OHCs (1.21 ± 0.2) ($P = 0.99$, $t = 0.01337$ df = 16).

To summarize, despite the presumed absence of synaptic function in $\alpha9^{\Delta/\Delta}$ OHCs, the ultrastructure of efferent synapses was not significantly different from that of wild-type littermates. In fact, although highly variable, some cisterns had an enlarged lumen equivalent to those of gain of function ($\alpha9^{L9'T/L9'T}$) hair cells.

SK2 knockout mice ($SK2^{\Delta/\Delta}$)

Among the genetically altered mice studied, knockout of the SK2 potassium channel causes the largest changes in efferent innervation. Efferent terminals are virtually absent from the apical cochlear turn (Kong et al., 2008), but a reduced number of efferent fibers remain in the high-frequency basal turn (Murthy et al., 2009a), and so were available for study by electron microscopy (5 in row 1, 6 in row 2, 5 in row 3). Consistent with diminished innervation, efferent contacts were reduced in $SK2^{\Delta/\Delta}$ cross sections; only four efferent terminals on 16 OHCs were found in 385 sections, compared with eight terminals on 6 OHCs in 154 sections from wild-type littermates. Another 15 small synaptic cisterns were found in $SK2^{\Delta/\Delta}$ OHCs opposing empty space with no efferent terminal in sight (Fig. 8A). In two instances what appeared to be the remains of a degenerated efferent terminal were seen. Whether associated with efferent terminals or not, synaptic cisterns were on average smaller in maximum extent (0.85 μm, from individual sections) than those of homozygous wild-type OHCs (2.5 μm). Synaptic cisterns in the $SK2^{\Delta/\Delta}$ OHCs were notably thinner, and

occasionally lacking a visible lumen, as though the cisternal membranes had fused (Fig. 8B). The cytoplasmic gap was 14.2 ± 2.0 nm wide (n = 20). The cisternal lumen averaged 16 ± 3.0 nm in width. The cistern to cytoplasmic gap volume ratio was 1.15 in the $SK2^{\Delta/\Delta}$ OHCs, smaller but not significantly (P = 0.11, t = 1.673 df = 28) different from that of OHCs in homozygous wild-type littermates (1.39) (Fig 3).

To summarize, many fewer efferent synapses were found in basal turn OHCs of $SK2^{\Delta/\Delta}$ mice. Synaptic cisterns were smaller than in control, and could be found with or without accompanying efferent synaptic terminals. In fact, a majority of cisterns in $SK2^{\Delta/\Delta}$ OHCs faced empty extracellular space, in two instances containing what appeared to be a degenerating neural process.

Afferent synapses in $SK2^{\Delta/\Delta}$ OHCs

In contrast to the paucity of efferent synapses, afferent synaptic structures were observed more frequently in $SK2^{\Delta/\Delta}$ OHCs than in other OHCs. Twelve active zones (ribbons) at 16 afferent contacts were observed in 200 sections covering 16 $SK2^{\Delta/\Delta}$ OHCs (some afferent contacts did not include active zones). In all other OHCs, wild-type and transgenic combined, including 1,300 serial sections covering 54 OHCs, only 11 active zones were observed at 16 afferent contacts. Afferent contact area was significantly greater in $SK2^{\Delta/\Delta}$ OHCs than in : all other OHCs (Table 2). The dense bodies (ribbons) in $SK2^{\Delta/\Delta}$ OHCs were larger as well (Fig. 9), extending through 5.6 sections on average, (compared with 3.5 sections in other OHCs), so that total volume of the dense bodies was twice that of other OHCs, although this difference just missed statistical significance. These larger ribbons were associated with greater numbers of vesicles on average (Fig. 9), but with a wide range of variability (Table 2). As in other OHCs, vesicles in $SK2^{\Delta/\Delta}$ OHCs were irregular in size, shape, and spatial distribution (Fig. 9). Organized “halos” of similarly sized vesicles like those found in inner hair cells (Weisz et al., 2012) were not seen in $SK2^{\Delta/\Delta}$, or any wild-type OHCs.

DISCUSSION

The synaptic cistern that lies in apposition to efferent contacts on OHCs has inspired speculation about its function for many years. A frequent suggestion is that the cistern serves as a calcium store activated by AChR gating, and pharmacological tests provide some support for this idea (Evans et al., 2000; Lioudyno et al., 2004; Sridhar et al., 1997). In contrast, the voltage dependence (Martin and Fuchs, 1992) and time course of efferent-evoked synaptic currents (Oliver et al., 2000) is best explained as resulting from calcium influx into the restricted diffusion space between the plasma membrane and cisternal membrane. Alternatively, then, the cistern’s primary role may be that of a barrier or fixed buffer to segregate synaptic calcium signals. The present study details cisternal structure in OHCs of mice with genetically altered function to gain insight into this question.

Several aspects of cistern structure were common to all mouse strains examined. With the exception of $SK2^{\Delta/\Delta}$ mice (in which efferent terminals are much reduced in number and size), the synaptic cisterns were coextensive with the efferent synaptic contacts. A single continuous cistern usually spanned adjacent efferent terminals, exceeding 3 μm in maximal

extent. Efferent terminals were richly endowed with synaptic vesicles that clustered toward numerous presumptive active zones. These active zones were found throughout the ending, rather than restricted to a central pocket. A coextensive cistern may be required to deal with transmitter release as it occurs anywhere throughout the relatively large synaptic contact.

In all OHCs, the adjacent cisternal membrane formed a virtually unbroken line 14 nm from the plasma membrane, with little variation throughout its microns-long extent. Similarly regular spacing has been reported for the “subsurface cisterns” found in muscle and neurons (Henkart et al., 1976) as well as in OHCs of guinea pigs (Smith and Sjostrand, 1961b). As reported then and observed presently as well, the narrow gap between the cisternal and plasma membrane has heterogeneous staining, indicating structures that might provide the remarkable regularity of this connection. An initial motivation for the present work was the suspicion that cisternal disposition might be altered if AChRs or associated channels were dysfunctional. However, this suspicion was not supported, because cisternal connections to the plasma membrane were similar in all genetically altered and wild-type mouse synapses. Furthermore, the $SK^{\Delta/\Delta}$ deletion eliminates protein expression (Bond et al., 2004), and the $\alpha9^{\Delta/\Delta}$ deletion removes all transmembrane segments (Vetter et al., 1999). Consequently, one can also conclude that other, yet to be identified, proteins comprise the cisternal connections.

Membrane bounding the far (cytoplasmic) side of the cistern was variable in appearance, sometimes parallel, but frequently bulging toward the cytoplasmic center. Some of these bulges became membranous vesicles with narrowed connections to the cistern in succeeding sections. In some instances, a second cistern, parallel to first and with a similar lumen, was observed. Variability in appearance of the cytoplasmic membrane of the cistern was noted as well in an earlier study of efferent synapses on guinea pig OHCs in which the membrane was described as “more delicate, almost beaded in character” (Smith and Sjostrand, 1961b). One possibility is that these irregularities of the membrane occur because the cytoplasmic surface of the synaptic cistern buds off calcium-loaded vesicles for transfer to nearby cellular organelles. Mitochondria occur in close contact with the synaptic cistern, and the OHC nucleus often approaches within 100 nm.

Even with the irregular shape of the cytoplasmic surface, the cisternal lumen averaged 18 nm in width among wild-type OHCs, including connected vesicles. Consequently, the normal cisternal volume is only 29% larger than the cytoplasmic volume formed between the cistern and the plasma membrane, suggesting limited storage capacity. How does this compare with known functional calcium stores? In ventricular myocytes the junctional sarcoplasmic reticulum volume is 350% that of the dyadic space into which calcium flows through voltage-gated calcium channels (Li et al., 2011). Even if it contained a high-capacity buffer such as sarcoplasmic calsequestrin, these relative volumes suggest that the hair cell’s synaptic cistern would be a minor contributor of calcium by comparison with the reliance on stored calcium in muscle.

A second consideration is the gap volume itself, which serves as a restricted diffusion space for calcium entering through activated α9α10 AChRs. An earlier model (Martin and Fuchs, 1992) suggested that calcium could rise to near 100 μM in the cytoplasmic gap during

cholinergic transmission. This model assumed free diffusion within the gap and out to the bulk cytoplasm. However, the real distribution is undoubtedly more restricted. Entering calcium is unlikely to diffuse freely, given the many connecting proteins that populate the cytoplasmic space between plasma and cisternal membranes. Instead, the rapid decay of synaptic potassium currents and the ability of the hair cell to respond repeatedly to efferent release imply that calcium rises instantaneously to locally high levels, and is then removed rapidly from the subcisternal space. The obvious exit for calcium is into the cistern, but whether that occurs by active transport, or by some form of calcium pore, is unknown.

Cisternal dimensions were generally similar between genetically altered and wild-type OHCs. Two exceptions were the diminished cisterns of the $SK2^{\Delta/\Delta}$ OHCs, and enlarged cisterns of $\alpha9^{L9'T/L9'T}$ (knockin) OHCs. Given the degenerated efferent innervation of the $SK2^{\Delta/\Delta}$, changes in synaptic ultrastructure could be a general consequence, rather than a specific influence of SK channels at the synapse. At the same time, this result complements observations of development of efferent contacts on inner hair cells, in which SK channel expression is tightly correlated with the appearance of AChR clusters and spontaneous synaptic activity in inner hair cells (Roux et al., 2011). The retraction of efferent synaptic contacts and shrinking of the synaptic cisterns in $SK2^{\Delta/\Delta}$ OHCs, but not in $\alpha9^{\Delta/\Delta}$ OHCs, implies that efferent excitation only (i.e., AChRs without SK channels), as opposed to absent activity, is particularly detrimental to the establishment and stabilization of these synaptic contacts. At the same time, these cells also lack the SK2 protein, which loss itself, rather than a specific change in activity, might destabilize synaptic structure. A nonconducting, but structurally normal SK2 variant would provide some insight into this distinction.

The larger cisternal volume observed in $\alpha9^{L9'T/L9'T}$ OHCs with enhanced cholinergic activity (Taranda et al., 2009) supports the possibility that the cistern serves primarily as a sink for efferent calcium influx, absorbing and shuttling calcium away from the plasma membrane. Calcium transport via budded cisternal vesicles would prevent interference with other calcium-dependent processes, such as transmitter release from nearby ribbon synapses. In contrast, normally sized cisterns in the $\alpha9^{\Delta/\Delta}$ OHCs argue against an exclusive role for efferent activity per se in determining cisternal volume. $\alpha9^{\Delta/\Delta}$ mice lack efferent suppression of cochlear distortion products and compound action potentials (Vetter et al., 1999). However, direct measurement of the cholinergic response in these OHCs has not been made. It remains possible, although perhaps unlikely, that some form of ACh-evoked calcium influx persists in these cells. A stronger possibility is that the synaptic cistern not only buffers calcium flux through AChRs, but also prevents calcium entry at nearby ribbon synapses from spreading to the efferent synapse. Such a dual role would have great utility. Activation of nearby SK2 channels by voltage-gated calcium signals at the ribbon synapse would seriously degrade afferent signaling, hyperpolarizing the membrane with a time course far longer than that of acoustic receptor potentials. Likewise, calcium entering through AChRs to inhibit the OHC should not be allowed to evoke afferent transmitter release. Blockade of SERCA pumps (sarco-endoplasmic reticulum calcium-ATPase) enhances voltage-gated calcium activation of SK2 current in turtle hair cells (Tucker and Fettiplace, 1996), consistent with the hypothesis that an endoplasmic cistern normally segregates these activities.

Finally, efferent synapses on immature inner hair cells also include small synaptic cisterns, although here the much larger voltage-gated calcium currents readily activate SK2 channels (Kong et al., 2008; Marcotti et al., 2004). It is of interest to consider whether developmental interactions between efferent and afferent synaptic contacts might be mediated somehow by the synaptic cistern. For example, efferent quantum content (synaptic strength) increases when hair cell calcium rises (Kong et al., 2012). Nitric oxide serves as the retrograde messenger whose synthesis can be increased by voltage-gated calcium influx, or by release from internal stores. Thus, the developmental halt of calcium-spiking and downregulation of calcium current (Beutner and Moser, 2001; Marcotti et al., 2003) may trigger attendant changes in efferent synaptic strength. The synaptic cistern is positioned to serve as an integrator of cellular activity, a starting point for second-messenger-mediated cascades during maturation of inner hair cells, and a physical arbiter of calcium-dependent synaptic activity in OHCs.

Acknowledgments

Grant sponsor: National Institute on Deafness and Other Communication Disorders, National Institutes of Health; Grant numbers: R01 DC001508; P30 DC005211.

LITERATURE CITED

Beutner D, Moser T. The presynaptic function of mouse cochlear inner hair cells during development of hearing. J Neurosci. 2001; 21:4593–4599. [PubMed: 11425887]

Bond CT, Herson PS, Strassmaier T, Hammond R, Stackman R, Maylie J, Adelman JP. Small conductance Ca2+-activated K+ channel knock-out mice reveal the identity of calcium-dependent after hyperpolarization currents. J Neurosci. 2004; 24:5301–5306. [PubMed: 15190101]

Dulon D, Luo L, Zhang C, Ryan AF. Expression of small-conductance calcium-activated potassium channels (SK) in outer hair cells of the rat cochlea. Eur J Neurosci. 1998; 10:907–915. [PubMed: 9753158]

Elgoyhen AB, Johnson DS, Boulter J, Vetter DE, Heinemann S. Alpha 9: an acetylcholine receptor with novel pharmacological properties expressed in rat cochlear hair cells. Cell. 1994; 79:705–715. [PubMed: 7954834]

Elgoyhen AB, Vetter DE, Katz E, Rothlin CV, Heinemann SF, Boulter J. alpha 10: a determinant of nicotinic cholinergic receptor function in mammalian vestibular and cochlear mechanosensory hair cells. Proc Natl Acad Sci USA. 2001; 98:3501–3506. [PubMed: 11248107]

Engstrom H. On the double innervation of the sensory epithelia of the inner ear. Acta Otolaryngol. 1958; 49:109–118. [PubMed: 13532652]

Evans MG, Lagostena L, Darbon P, Mammano F. Cholinergic control of membrane conductance and intracellular free Ca2+ in outer hair cells of the guinea pig cochlea. Cell Calcium. 2000; 28:195–203. [PubMed: 11020381]

Fiala JC. Reconstruct: a free editor for serial section microscopy. J Microsc. 2005; 218:52–61. [PubMed: 15817063]

Heinzeller T, Tutter I. Pinealocyte subsurface cisterns. II: Influence of time of day, sympathectomy, and castration. J Pineal Res. 1991; 10:84–90. [PubMed: 2056438]

Henkart M, Landis DM, Reese TS. Similarity of junctions between plasma membranes and endoplasmic reticulum in muscle and neurons. J Cell Biol. 1976; 70:338–347. [PubMed: 939781]

Kaufmann WA, Ferraguti F, Fukazawa Y, Kasugai Y, Shigemoto R, Laake P, Sexton JA, Ruth P, Wietzorrek G, Knaus HG, Storm JF, Ottersen OP. Large-conductance calcium-activated potassium channels in purkinje cell plasma membranes are clustered at sites of hypolemmal microdomains. J Comp Neurol. 2009; 515:215–230. [PubMed: 19412945]

Kong JH, Adelman JP, Fuchs PA. Expression of the SK2 calcium-activated potassium channel is required for cholinergic function in mouse cochlear hair cells. J Physiol. 2008; 586:5471–5485. [PubMed: 18818242]

Kong JH, Zachary S, Rohmann KN, Fuchs PA. Retrograde facilitation of efferent synapses on cochlear hair cells. J Assoc Res Otolaryngol. 2012; 14:17–27. [PubMed: 23183877]

Lee DJ, Benson TE, Brown MC. Diverse synaptic terminals on rat stapedius motoneurons. J Assoc Res Otolaryngol. 2008; 9:321–333. [PubMed: 18563488]

Li L, Louch WE, Niederer SA, Andersson KB, Christensen G, Sejersted OM, Smith NP. Calcium dynamics in the ventricular myocytes of SERCA2 knockout mice: A modeling study. Biophys J. 2011; 100:322–331. [PubMed: 21244828]

Lioudyno M, Hiel H, Kong JH, Katz E, Waldman E, Parameshwaran-lyer S, Glowatzki E, Fuchs PA. A “synaptoplasmic cistern” mediates rapid inhibition of cochlear hair cells. J Neurosci. 2004; 24:11160–11164. [PubMed: 15590932]

Marcotti W, Johnson SL, Rusch A, Kros CJ. Sodium and calcium currents shape action potentials in immature mouse inner hair cells. J Physiol. 2003; 552:743–761. [PubMed: 12937295]

Marcotti W, Johnson SL, Kros CJ. A transiently expressed SK current sustains and modulates action potential activity in immature mouse inner hair cells. J Physiol. 2004; 560:691–708. [PubMed: 15331671]

Martin AR, Fuchs PA. The dependence of calcium-activated potassium currents on membrane potential. Proc R Soc Lond B Biol Sci. 1992; 250:71–76.

Murthy V, Maison SF, Taranda J, Haque N, Bond CT, Elgoyhen AB, Adelman JP, Liberman MC, Vetter DE. SK2 channels are required for function and long-term survival of efferent synapses on mammalian outer hair cells. Mol Cell Neurosci. 2009a; 40:39–49. [PubMed: 18848895]

Murthy V, Taranda J, Elgoyhen AB, Vetter DE. Activity of nAChRs containing alpha9 subunits modulates synapse stabilization via bidirectional signaling programs. Dev Neurobiol. 2009b; 69:931–949. [PubMed: 19790106]

Nagy, Jl; Yamamoto, T.; Jordan, LM. Evidence for the cholinergic nature of C-terminals associated with subsurface cisterns in alpha-motoneurons of rat. Synapse. 1993; 15:17–32. [PubMed: 8310422]

Oliver D, Klocker N, Schuck J, Baukrowitz T, Ruppersberg JP, Fakler B. Gating of Ca2+-activated K+ channels controls fast inhibitory synaptic transmission at auditory outer hair cells. Neuron. 2000; 26:595–601. [PubMed: 10896156]

Omata T, Schatzle W. Electron microscopical studies on the effect of lapsed time on the nerve endings of the outer hair cells in acoustically exposed rabbits. Arch Otorhinolaryngol. 1984; 240:175–183. [PubMed: 6477295]

Orci L, Ravazzola M, Le Coadic M, Shen WW, Demaurex N, Cosson P. From the Cover: STIM1-induced precorneal and cortical subdomains of the endoplasmic reticulum. Proc Natl Acad Sci U S A. 2009; 106:19358–19362. [PubMed: 19906989]

Plazas PV, De Rosa MJ, Gomez-Casati ME, Verbitsky M, Weisstaub N, Katz E, Bouzat C, Elgoyhen AB. Key roles of hydrophobic rings of TM2 in gating of the alpha9alpha10 nicotinic cholinergic receptor. Br J Pharmacol. 2005; 145:963–974. [PubMed: 15895110]

Roux I, Wersinger E, Mcintosh JM, Fuchs PA, Glowatzki E. Onset of cholinergic efferent synaptic function in sensory hair cells of the rat cochlea. J Neurosci. 2011; 31:15092–15101. [PubMed: 22016543]

Saito K. Fine structure of the sensory epithelium of the guinea pig organ of Corti: afferent and efferent synapses of hair cells. J Ultrastruct Res. 1980; 71:222–232. [PubMed: 7381992]

Smith C, Sjostrand F. A synaptic structure in the hair cells of the guinea pig cochlea. J Ultrastruct Res. 1961a; 5:184–192.

Smith CA, Sjostrand FS. A synaptic structure in the hair cells of the guinea pig cochlea. J Ultrastruct Res. 1961b; 5:182–192.

Sridhar TS, Brown MC, Sewell WF. Unique postsynaptic signaling at the hair cell efferent synapse permits calcium to evoke changes on two time scales. J Neurosci. 1997; 17:428–437. [PubMed: 8987768]

Taranda J, Maison SF, Ballestero JA, Katz E, Savino J, Vetter DE, Boulter J, Liberman MC, Fuchs PA, Elgoyhen AB. A point mutation in the hair cell nicotinic cholinergic receptor prolongs cochlear inhibition and enhances noise protection. PLoS Biol. 2009; 7:e18. [PubMed: 19166271]

Tucker TR, Fettiplace R. Monitoring calcium in turtle hair cells with a calcium-activated potassium channel. J Physiol. 1996; 494:613–626. [PubMed: 8865061]

Tutter I, Heinzeller T, Aschauer B. Pinealocyte subsurface cisterns. I: Cytological aspects including three-dimensional structure. J Pineal Res. 1991a; 10:74–83. [PubMed: 2056437]

Tutter I, Heinzeller T, Seitz-Tutter D. Pinealocyte subsurface cisterns. Ill: Storage of calcium ions and their probable role in cell stimulation. J Pineal Res. 1991b; 10:91–99. [PubMed: 2056439]

Vetter DE, Liberman MC, Mann J, Barhanin J, Boulter J, Brown MC, Saffiote-Kolman J, Heinemann SF, Elgoyhen AB. Role of alpha9 nicotinic ACh receptor subunits in the development and function of cochlear efferent innervation. Neuron. 1999; 23:93–103. [PubMed: 10402196]

Weisz CJ, Lehar M, Hiel H, Glowatzki E, Fuchs PA. Synaptic transfer from outer hair cells to type II afferent fibers in the rat cochlea. J Neurosci. 2012; 32:9528–9536. [PubMed: 22787038]

Wersinger E, Fuchs PA. Modulation of hair cell efferents. Hear Res. 2011; 279:1–12. [PubMed: 21187136]

Yamamoto T, Hertzberg EL, Nagy Jl. Subsurface cisterns in alpha-motoneurons of the rat and cat: immunohistochemical detection with antibodies against connexin32. Synapse. 1991; 8:119–136. [PubMed: 1652794]

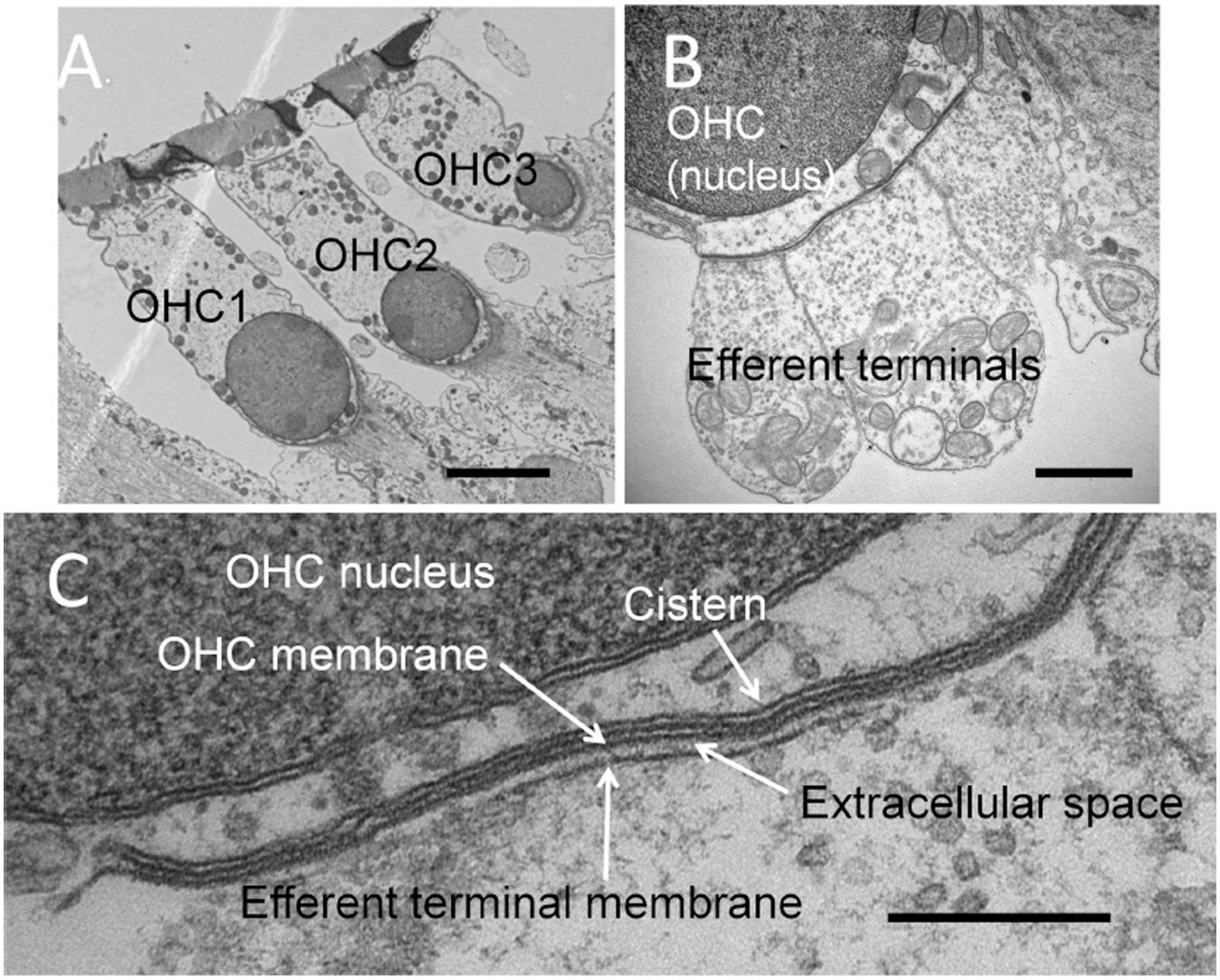

Figure 1.

Efferent synapses on wild-type outer hair cells (OHCs). **A:** Low-power cochlear cross section showing OHCs from three rows (OHC1-3). **B:** Higher power view of multiple efferent terminals on one wild-type OHC. **C:** High magnification showing parallel membranes that demarcate the synaptic cistern in apposition to an efferent terminal. Scale bar = 4 μm in A; 1 μm in B; 250 nm in C.

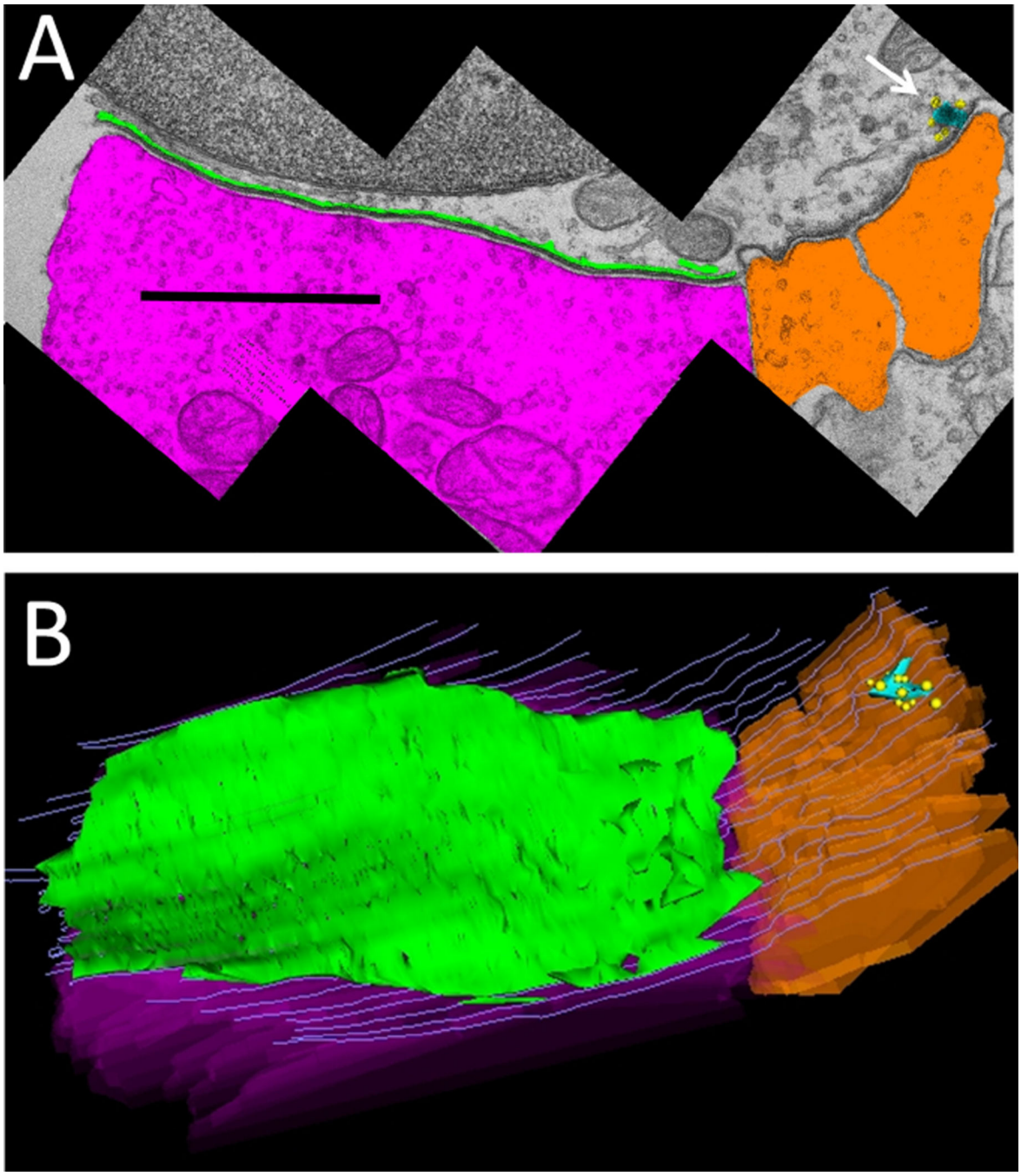

Figure 2.

Demarcation and reconstruction of efferent synapse on a wild-type OHC ($\alpha 9^{L9/L9}$). **A:** Single cross section. Efferent terminal in magenta, afferent boutons in umber, synaptic cistern in green, ribbon in turquoise, and ribbon-associated vesicles in yellow. White arrow points to synaptic ribbon **B:** Z-axis projection (tilted forward ~30 degrees from the plane of section) from a 3D reconstruction of 29 sections including that in A (same scale). Same color scheme as in A, with hair cell membrane shown in gray lines. Scale bar = 1 μm in A.

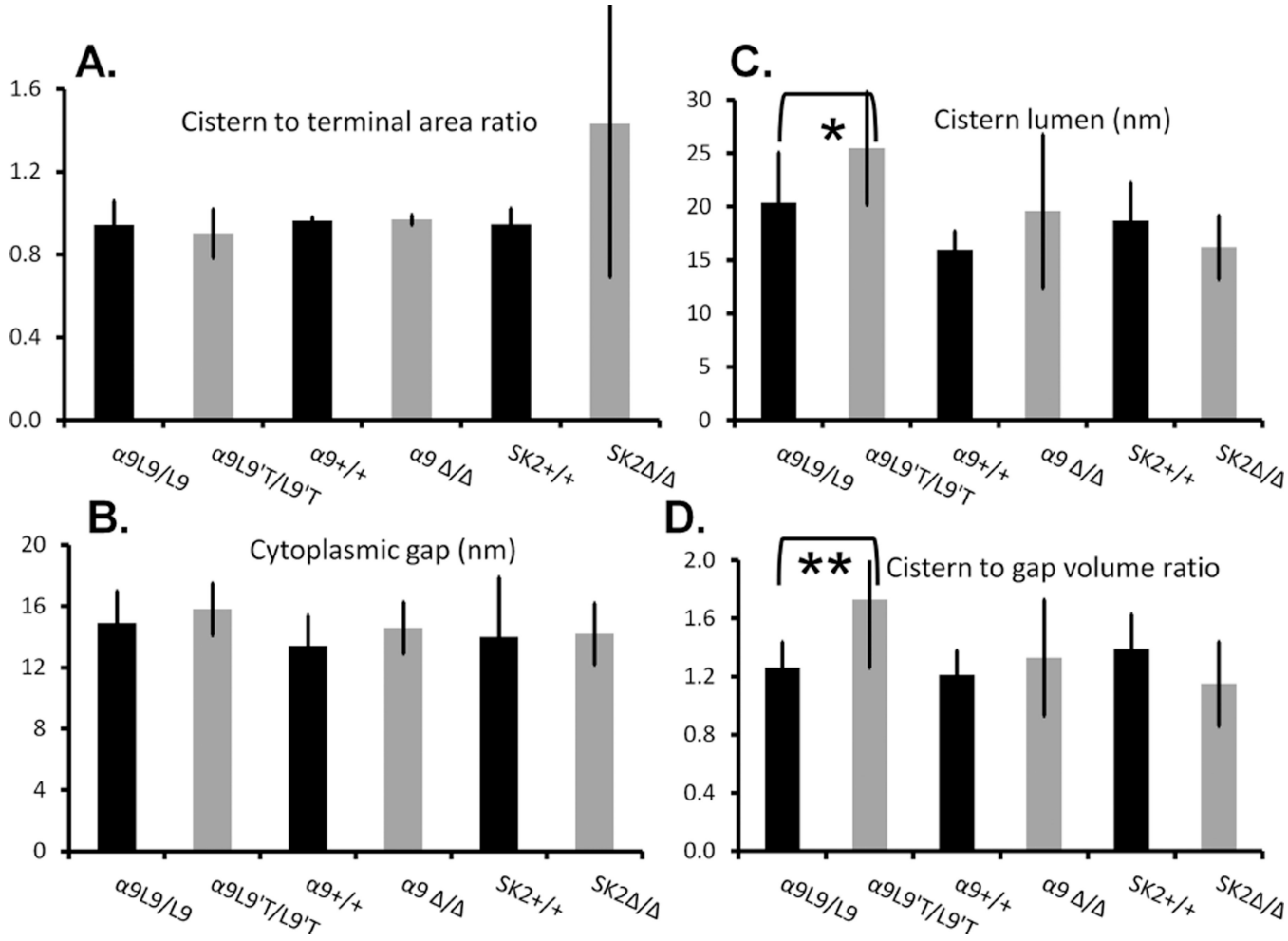

Figure 3.

Dimensions of synaptic cisterns in mouse outer hair cells. **A:** The ratio of appositional area of the cistern and efferent terminal. In all but the $SK2^{\Delta/\Delta}$ mice, cisterns and efferent terminals were coextensive. **B:** The average distance (in nm) of the cistern from the hair cell plasma membrane (obtained as the width of the 3D gap volume). **C:** The average lumen of the cistern (nm) obtained as the width of the 3D volume. **D:** Ratio of the cisternal volume to that of the cytoplasmic gap between the cistern and the hair cell plasma membrane.

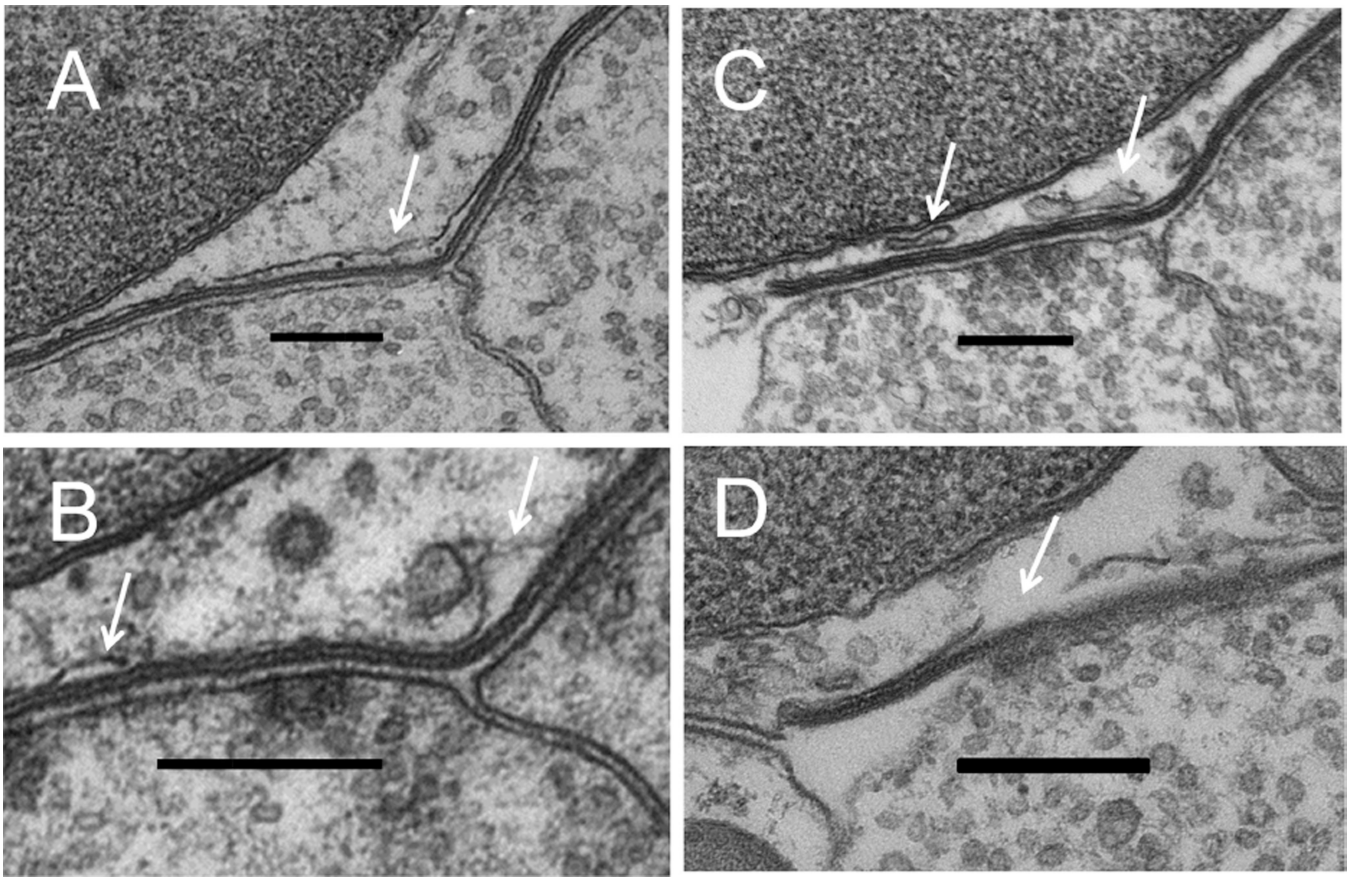

Figure 4.

Variations in cisternal structure. **A:** Enlargement of cistern at junction of two efferent terminals. **B:** Cisternal bulges. **C:** Accessory cisterns. **D:** Incomplete cisternal membrane. White arrows in each panel point to named objects. Scale bar = 300 nm in A–D.

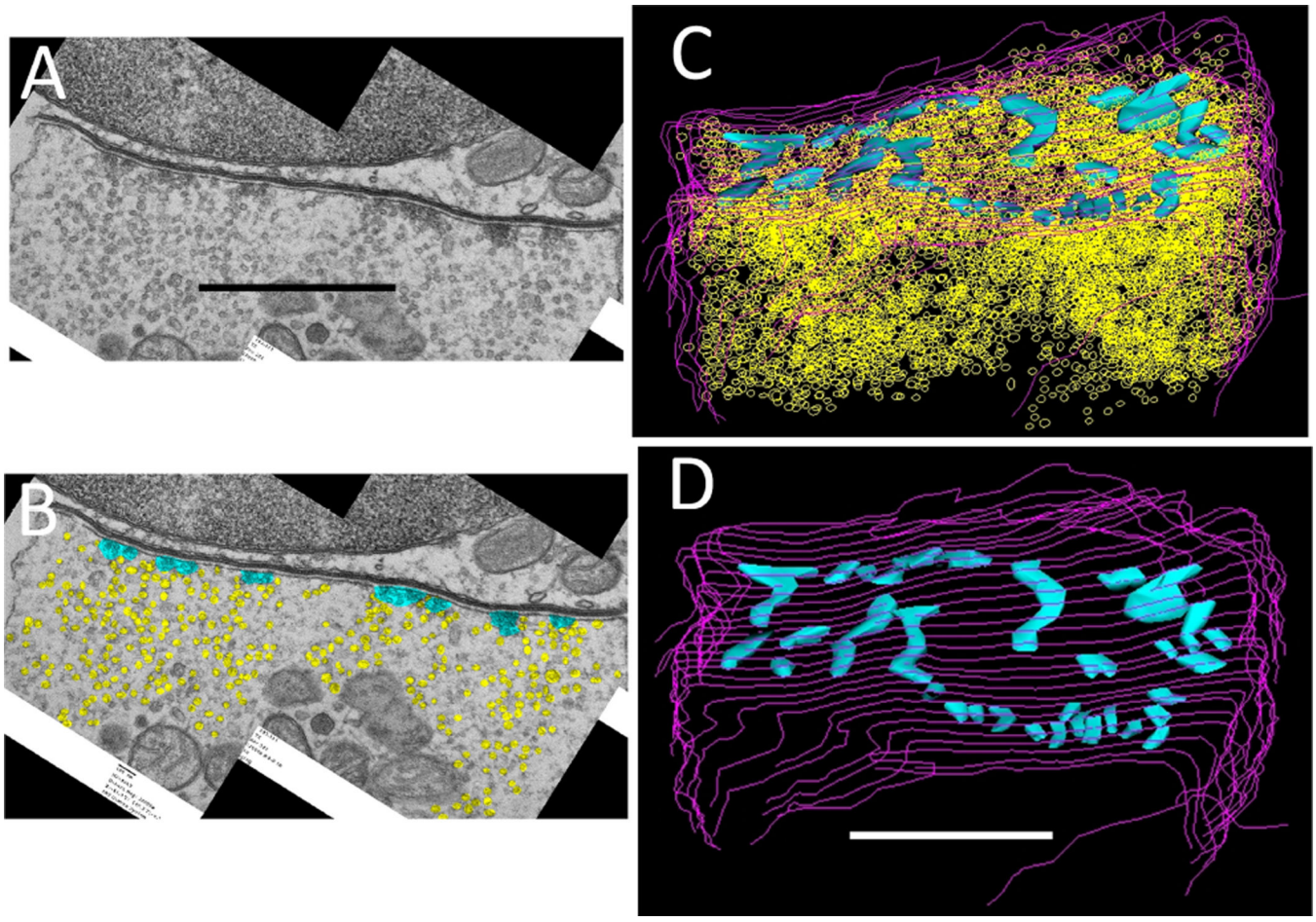

Figure 5.

Vesicles and active zones in an efferent terminal (same synapse as in Fig. 2). **A:** Single cross section. **B:** Vesicles (yellow) and active zones (turquoise) demarcated in same section as A. **C:** Z-axis projection (tilted forward 30 degrees from the plane of section) from 3D reconstruction of 27 serial sections including that in A and B. In all, 3,517 vesicles (yellow) populate these efferent terminal sections. **D:** Small clusters of vesicles and associated dense materials were outlined to indicate 31 active zones (turquoise) scattered throughout the efferent ending (approximately same orientation as C, without vesicles). Scale bar = 1 μm in A (applies to A,B) and D (applies to C,D).

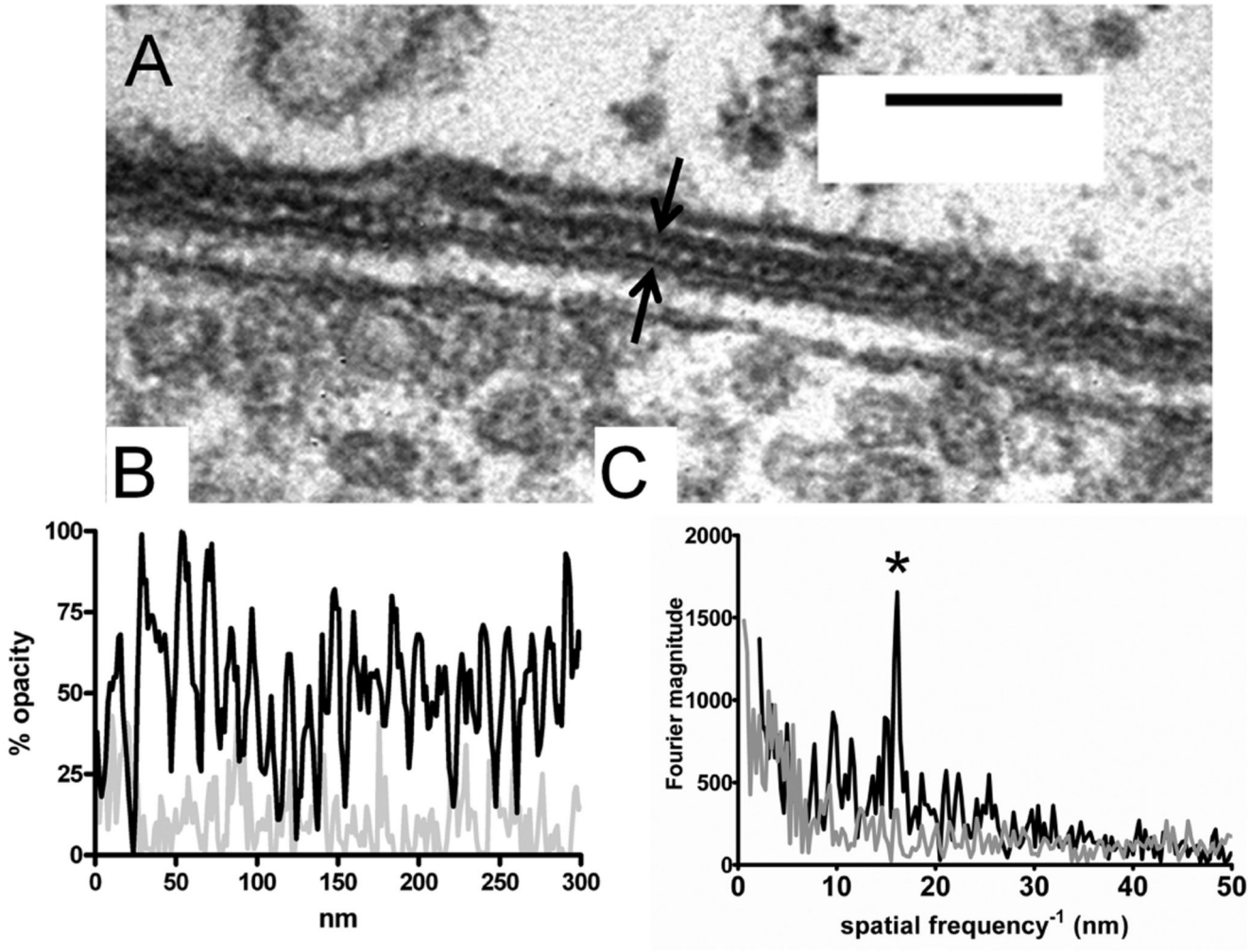

Figure 6.

A: High magnification of cytoplasmic gap between cistern and hair cell plasma membrane; vesicles in efferent terminal are seen in lower part of image. The cytoplasmic gap (bracketed by black arrows) contains semiperiodic densities. **B:** "Opacity profile" of a 300-nm line through the cytoplasmic gap (dark line). The light gray line shows the same analysis carried out in a nearby region of hair cell cytoplasm. **C:** Fourier analysis of opacity profiles from B. The cytoplasmic gap profile (black line) shows a prominent peak at a position corresponding to a 16-nm interval (asterisk). Nearby cytoplasm (gray line) had no such peak. Scale bar = 100 nm in A.

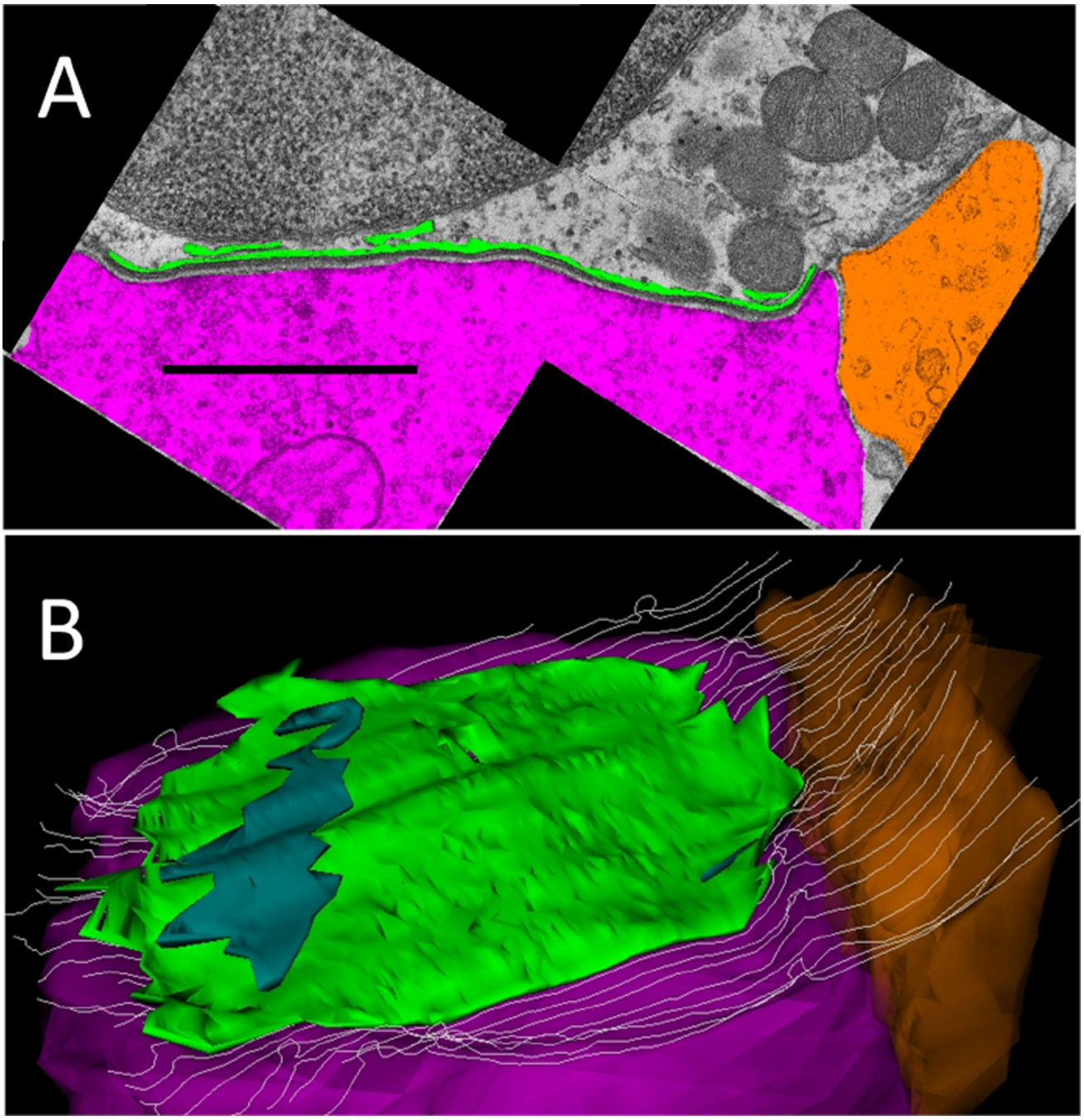

Figure 7.

Demarcation and reconstruction of an efferent synapse on an $\alpha 9^{L9'T/L9'T}$ (homozygous knockin) OHC. **A:** Cross-section montage. Efferent terminal in magenta, afferent bouton in umber, and cistern in green. **B:** Z-axis projection (tilted forward 30 degrees from the plane of section) from 3D reconstruction of 35 sections including that in A. Same color scheme. The largest of several secondary cisterns is in dark green. Scale bar = 1 μm in A.

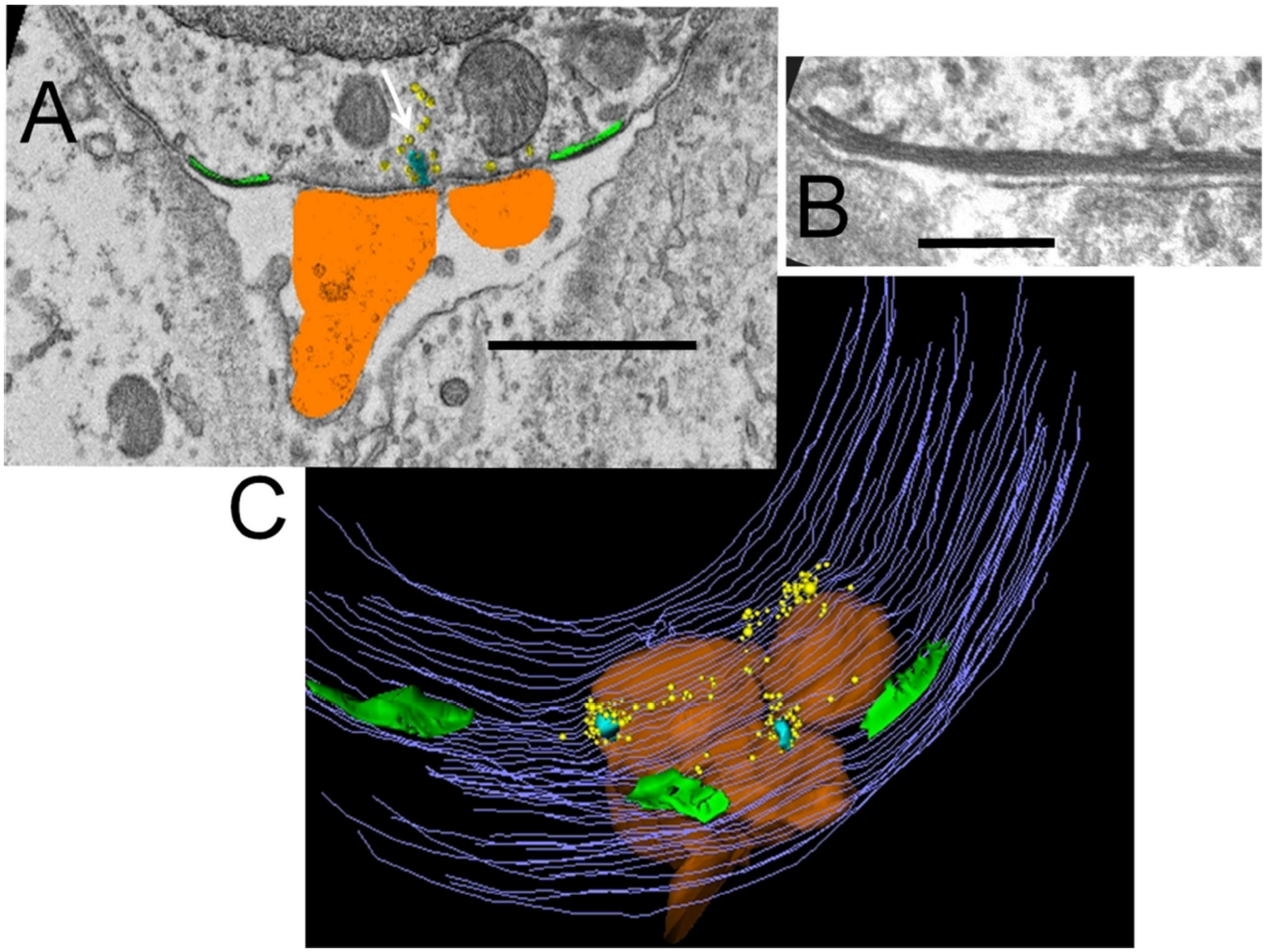

Figure 8.

Demarcation and reconstruction of the synaptic zone in an $SK2^{\Delta/\Delta}$ (homozygous knockout) OHC. **A:** Single section, cisterns in green, afferents in umber, ribbon in turquoise (white arrow), and synaptic vesicles in yellow. **B:** Close-up of cistern with partially fused lumen. **C:** Z-axis projection (tilted forward 30 degrees from the plane of section) from reconstruction of 46 sections including that in A. Same color scheme as in A; hair cell membrane is in gray. Scale bar = 1 μm in A; 120 nm in B.

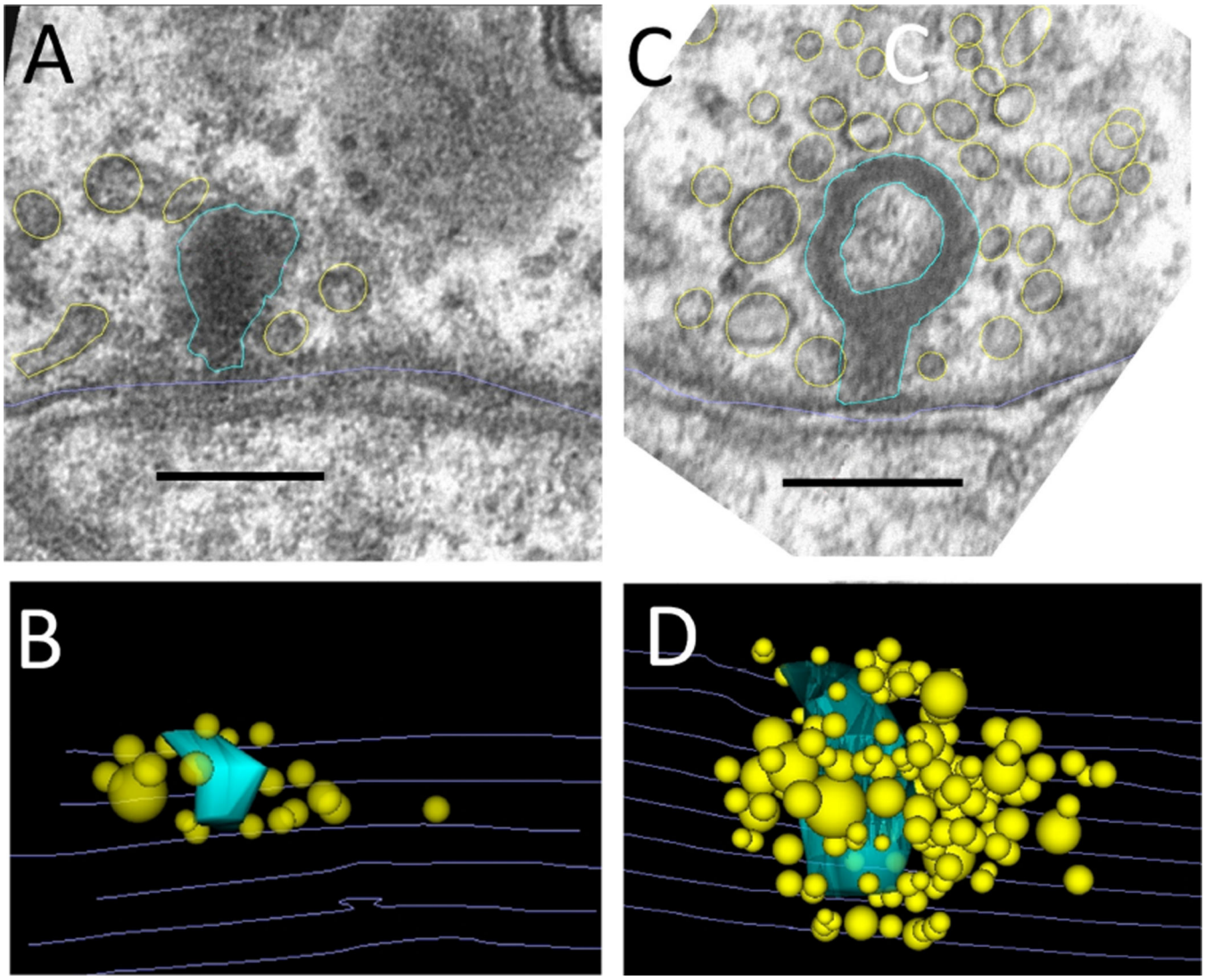

Figure 9.

Active zones in $SK2^{+/+}$ and $SK2^{\Delta/\Delta}$ OHCs. **A:** Exemplar cross section from an $SK2^{+/+}$ OHC (homozygous wild-type littermate). **B:** Z-axis projection (tilted forward 60 degrees from the plane of section) from 3D reconstruction using six sections including that in A. The dense body is turquoise, vesicles in yellow, hair cell membrane in gray. **C:** Exemplar cross section from an $SK2^{\Delta/\Delta}$ OHC. **D:** Z-axis projection (tilted forward 90 degrees from the plane of section) from 3D reconstruction using eight sections including that in C; same colors as in B. Scale bar = 200 nm in A and C.

TABLE 1

Mouse Lines and Data Sets[1]

Genotype	Background	No. of animals	No. of cells	No. of synapses	total depth (μm)
Wild type					
$\alpha9^{L9/L9}$ (mid)	FVB129.J2 (agouti)	2	8	10	15.8
$\alpha9^{+/+}$ (mid)	129S6 x CBA/CaJ	1	5	5	2.3
$SK2^{+/+}$ (base)	C57BI/6 (black)	1	5	8	10.3
Total		**4**	**18**	**23**	28.4
Altered					
$\alpha9^{L9'T/L9'T}$ (mid)	FVB129.J2 (agouti)	2	20	22	23.1
$\alpha9^{\Delta/\Delta}$ (mid)	129S6 x CBA/CaJ	2	16	16	32.7
$SK2^{\Delta/\Delta}$ (base)	C57BI/6 (black)	2	16	20	13.3
Total		**6**	**52**	**58**	69.1

[1] Homozygous α9 knockin mice ($\alpha9^{L9'T/L9'T}$) and homozygous wild-type littermates ($\alpha9^{L9/L9}$), homozygous α9 knockout mice ($\alpha9^{\Delta/\Delta/}$) and their homozygous wild-type littermates ($\alpha9^{+/+}$), and homozygous SK2 knockout mice ($SK2^{\Delta/\Delta}$) and their homozygous wild-type littermates ($SK2^{+/+}$) were employed in this study.

TABLE 2

Ribbon Synapses in $SK2^{\Delta/\Delta}$ Compared With All Other Outer Hair Cells (OHCs)[1]

	$SK^{\Delta/\Delta}$ OHCs	All other OHCs	*P* value
Afferent contact (μm)	1.85 ± 0.38	1.01 ± 0.39	<0.001
Dense body volume (μm^3)	0.0062 ± 0.0013	0.0029 ± 0.0010	0.07
Vesicles	32.1 ± 15.9	23.3 ± 12.6	0.19
Sections	5.6 ± 1.5	3.5 ± 1.4	<0.001

[1]Comparison of afferent synaptic contacts in all wild-type OHCs versus $SK2^{\Delta/\Delta}$ OHCs. Afferent contact is the greatest length of afferent to hair cell contact in each serial reconstruction (n = 16 afferent contacts in each column). Twelve active zones (dense bodies with vesicles) in $SK2^{\Delta/\Delta}$ and 11 active zones in all other OHCs were analyzed. Ribbon volume was obtained from 3D reconstruction, and multiple ribbons at single active zones were summed. Vesicle numbers report the average number of vesicles within 1 urn of each reconstructed ribbon. Section number is the number of sections included in the 3D reconstruction of each active zone. Ribbons were more frequent and more extensive in $SK2^{\Delta/\Delta}$ OHCs than in other OHCs. Mean ± standard deviation is given in all cases. Statistical significance was established by two-tailed unpaired *t*-test.